Cancer Science
Japanese Cancer Association JCA
Open Access

Peptide-based tumor inhibitor encoding mitochondrial p14^{ARF} is highly efficacious to diverse tumors

Ken Saito,[1] Hidekazu Iioka,[1] Chie Kojima,[2] Mikako Ogawa[3] and Eisaku Kondo[1]

[1]Division of Molecular and Cellular Pathology, Niigata University Graduate School of Medical and Dental Sciences, Niigata; [2]Department of Applied Chemistry, Graduate School of Engineering, Osaka Prefecture University, Osaka; [3]Laboratory of Bioanalysis and Molecular Imaging, Graduate School of Pharmaceutical Sciences, Hokkaido University, Sapporo, Japan

Key words
Mitochondria, p14, peptide, therapeutics, tumor suppressor

Correspondence
Eisaku Kondo, Division of Molecular and Cellular Pathology, Niigata University Graduate School of Medical and Dental Sciences, 1-757 Asahimachi-dori, Chuo-ku, Niigata 951-8510, Japan.
Tel: +81-25-227-2102; Fax: +81-25-227-0761;
E-mail: ekondo@med.niigata-u.ac.jp

Funding Information
Japan Society for the Promotion of Science (JSPS) (#25670263).

Received March 24, 2016; Revised June 7, 2016; Accepted June 10, 2016

Cancer Sci **107** (2016) 1290–1301

doi: 10.1111/cas.12991

***p14^{ARF}* is one of the major tumor suppressors conventionally identified both as the mdm2-binding molecule restoring *p53* function in the nucleus, and as a nucleophosmin-binding partner inside the nucleolous to stabilize ribosomal RNA. However, its recently reported mitochondrial localization has pointed to novel properties as a tumor suppressor. At the same time, functional peptides are gaining much attention in nanomedicine for their *in vivo* utility as non-invasive biologics. We previously reported the p14^{ARF}-specific peptide that restored the sensitivity to gefitinib on the gefitinib-resistant lung cancer cells. Based on the information of this prototype peptide, here we generated the more powerful anti-tumor peptide "r9-CatB-p14 MIS," which comprises the minimal inhibitory sequence of the mitochondrial targeting p14^{ARF} protein in combination with the proteolytic cleavage site for cathepsin B, which is activated in various tumor cells, fused with the nine-polyarginine-domain for cell penetration, and demonstrated its novel action of regulating mitochondrial function in accordance with localization of endogenous p14^{ARF}. The p14 MIS peptide showed a potent tumor inhibiton *in vitro* and *in vivo* against not only lung cancer cells but also tumor cells of diverse lineages, via modulating mitochondrial membrane potential, with minimal cytotoxicity to non-neoplastic cells and tissues. Hence, this mitochondrially targeted p14 peptide agent provides a novel basis for non-invasive peptide-based antitumor therapeutics.**

p14^{ARF} (*p19^{ARF}* in murine) is encoded by the CDKN2A locus on chromosome 9p21, which is generated by alternative splicing and shares with *p16^{INK4a}* two of the three exons on the locus;[1,2] the signaling pathway, however, is different from another major splicing variant, p16, as a cyclin (cdk4/6)-dependent kinase inhibitor. Because it is a nuclear (nucleolar and nucleoplasm) protein, the molecular function of *p14^{ARF}* is multimodal: for example, it interacts with Mdm2 to inhibit cell cycle progression through activation of p53, whereas in the nucleolus its interaction with B23/NPM inhibits ribosomal biogenesis through control of rRNA processing.[3,4] Furthermore, *p14^{ARF}* is an activator of DNA repair pathways in response to DNA damage.[5,6] Understanding these diverse physiologic functions, involving molecular "crosstalk" is complex, but it is known that *p14^{ARF}* participates in tumor suppression *in vivo*, as has been demonstrated by the tumor susceptibility phenotype of ARF-deficient mice.[7–9]

Many of these findings have been hitherto presented in the context of nuclear events for *p14^{ARF}*, but a close examination of the latest results increasingly reveals a new functionality: mitochondrial *p14^{ARF}*. It interacts with the mitochondrial protein p32/C1QBP, which is essential to ARF's pro-apoptotic function.[10] The hydrophobic domain within the amino-terminal half of p14^{ARF} serves as a mitochondrial import sequence, and it interacts with Bcl-XL and p32 in a p53-independent manner after mitochondrial entry.[11] Moreover, a heat shock protein, HSP70, is reported to mediate mitochondrial localization of p14^{ARF}, which triggers autophagy in response to cellular stress.[12] These data suggest that various mitochondrial molecules are related to the mitochondrial localization and critical function of p14^{ARF}, and implicate *p14^{ARF}* as a significant tumor suppressor, while also illustrating the complexity of mitochondrial p14^{ARF} regulation.

Here we report on, through direct evidence of mitochondrial p14^{ARF} activity in various human tumor lineages, the potent anti-tumor peptide "p14 MIS," which we generated based on the minimal functional amino acid sequence within the N-terminal mitochondrial targeting p14 region. Such minimization of the core sequence is evidently important for optimizing and enhancing the function of the antitumor peptide as demonstrated by p16INK4a MIS peptide.[13] We also highlight the utility of p14 MIS as a non-invasive growth inhibitor of a diversity of malignancies.

Materials and Methods

Cell lines. MMNK-1 cells (normal cholangiocytes), normal human dermal fibroblast (NHDF) cells and human cancer cell

lines were prepared as previously described.[14,15] Briefly, cells were maintained in RPMI 1640 containing 10% FBS with 100 unit/mL penicillin and 100 mg/mL streptomycin (Life Technologies, Tokyo, Japan) at 37°C with 5% CO_2. NuLi-1 cells (normal human bronchus cells), TIME cells (human microvascular endothelium cells) and human pancreatic duct epithelial cell (HPNE) cells were purchased from the American Type Culture Collection (ATCC) and cultured following the instructions. A hepatocellular carcinoma line, HAK-1B, and a lung adenocarcinoma line, PC-9, were kind gifts from Dr Yano (Department of Pathology, Kurume University) and Dr Kiura (Department of Respiratory Medicine, Okayama University), respectively.

Antibodies and reagents. The primary antibodies used in the present study were as follows: mouse anti-$p14^{ARF}$ monoclonal antibody (P2610; Sigma-Aldrich, St. Louis, MO, USA) for conventional immunofluorescence, rabbit anti-p14 polyclonal antibody (SAB4500073; Sigma-Aldrich) for immunoelectron microscopy, goat anti-HSP60 polyclonal antibody (Santa Cruz Biotechnology, Dallas, TX, USA) and rabbit anti-cleaved PARP polyclonal antibody (Cell Signaling Technology, Tokyo, Japan). Secondary antibodies were: Alexa Fluor 488-conjugated rabbit anti-mouse IgG (H+L) antibody for p14 detection (Thermo Fisher Scientific, Carlsbad, CA, USA), Cy3-labeled rabbit anti-goat IgG (H+L) antibody for HSP60 detection (Jackson ImmunoResearch, West Grove, PA, USA), Alexa Fluor 555-conjugated goat anti-rabbit IgG (H+L) antibody for cleaved PARP detection (Thermo Fisher Scientific). Dyes/indicators and related reagents were: Hoechst 33342 dye (Molecular Probes, Eugene, OR, USA), Mito Tracker Red CMXRos (Molecular Probes), Lyso Tracker Red Lysosomal Probe (Molecular Probes), CellLight Mitochondria-RFP (mitochondrial marker), CellLight Lysosomes-RFP (lysosomal marker), mitochondrial membrane potential indicator, JC-1 (ThermoFisher Scientific, Waltham, MA, USA), ROS detection agent, CellROX Deep Red reagent (ThermoFisher Scientific) and Cyclosporin A (Sigma-Aldrich, Tokyo, Japan).

Peptide synthesis. All peptides were synthesized at the laboratory of the division of life science, Sigma-Aldrich Japan by standard Fmoc chemistry on an ABI 433A Peptide Synthesizer (Applied Biosystems, Foster City, USA). FITC-labeled peptides were purified to HCl form by reverse-phase HPLC to >95% purity for both *in vitro* and *in vivo* applications. Peptide identities were confirmed by mass spectrometry.

Immunohistochemistry and immunofluorescence. Antigen retrieval of paraffin-embedded sections, immunohistochemistry and signal development were performed as described previously.[15] The primary antibodies for p14ARF and Ki-67 were diluted at 1:500 in CanGet signal solution (Toyobo, Tokyo, Japan), respectively. For immunofluorescence, cells grown in the chamberslides were fixed with PBS containing 4% paraformaldehyde, subjected to incubate with the indicated primary antibodies, then reacted with the fluorescence-labeled secondary antibodies after repeated washing.

Immunoelectron microscopy. The HeLa cell samples cultured on the gold disks were rapidly frozen in liquid propane at −175°C, then substituted with 0.2% glutaraldehyde in ethanol for 48 h, and dehydrated and infiltrated with a 50:50 mixture of ethanol and resin (LR white; London Resin, London, UK). Finally, samples were embedded and polymerized with fresh 100% resin, cut into ultra-thin sections and then placed on nickel grids. The grids were incubated with primary antibody (rabitt anti-$p14^{ARF}$ polyAb; Sigma-Aldrich Japan) at 4°C overnight, then incubated with the 10-nm gold particle-conjugated goat anti-rabbit Ab after several washings. They were stained with 2% uranyl acetate and with Lead stain solution (Sigma-Aldrich Japan). The grids were observed under a transmission electron microscope (JEM-1400Plus; JEOL, Tokyo, Japan) at an acceleration voltage of 80 kV. Digital images were taken with a CCD camera (VELETA; Olympus Soft Imaging Solutions GmbH, Münster, Germany).

Cell proliferation assay (MTT assay). Cells (1×10^4) were seeded on a 24-well plate. The next day, the medium was changed to fresh RPMI 1640 with 10% FBS, and cells were treated with 10 μM of p14 peptides and 5 μM of cyclosporin A for 48 h. Cell growth was measured using Cell Count Reagent SF (Nacalai Tesque, Kyoto, Japan) according to the manufacturer's protocol.

RT-PCR. Total RNA from each cell sample was isolated using RNeasy plus mini kit and oligo dT-primed cDNA were synthesized from total RNAs using the Super Script III kit (Life Technologies). Each cDNA was amplified by PCR with the following primer sets and Taq polymerase (z-Taq; Takara Bio, Tokyo, Japan). Primers for $p14^{ARF}$ were 5′-TGCTGATGCTAC TGAGGAGCC-3′ and 5′-CGCGGCCGCTCAGCCAGGTCCA CGGGCAGA-3′, for *ATPAF1* were 5′-GGCTCAGTCCTGTC-CAACAT-3′ and 5′-GTGCCTCAGCAACATTCAGA-3′, for *UCP-2* were 5′-CAAATGAGCTTTGCCTCTGTC-3′ and 5′-T CTGTCATGAGGTTGGCTTTC-3′, and for *Actin* were 5′-CC TCATGAAGATCCTCACCGA-3′ and Rv 5′-TGCCAATGGT GATGACCTGG-3′.

Detection of mitochondrial membrane potential. The cells were changed to medium containing 10 μg/mL concentration of JC-1 dye (ThermoFisher Scientific) and incubated at 37°C for 10 min before fluorescence measurement. After washing three times with fresh medium, red or green fluorescence on living cells was directly detected by inverted fluorescence microscopy (Olympus IX-71; Olympus, Tokyo, Japan).

Measurement of reactive oxygen species. Cells were seeded at a density of 1×10^4 cells/0.2 mL in 24-well dishes, then treated with the p14 peptides for 24 h. After washing with fresh medium, the cells were incubated with 5 μM of CellROX Deep Red reagent (ThermoFisher Scientific).

Animal models. A total of 2.0×10^6 cells of human pancreatic adenocarcinoma cells stably expressing green fluorescent protein (GFP-BxPC3) were transplanted into the peritoneal cavity of a 7-week-old NOD-SCID mouse by direct injection. A week after the tumor cell transplantation, mice were treated with the same dose of the i.p. injected r9-CatB-p14 MIS peptide or with polyarginines (r9) alone once per day for a regimen of 6 days (300 μg/dosage/mouse/day). Seven days after initial administration of the peptide, all mice were autopsied and their organs examined by fluorescence stereomicroscopy (Leica M165 FC; Leica Microsystems KK, Tokyo, Japan). The animal studies in the present work were approved by the Animal Research Committee of the Niigata University School of Medicine. All mouse procedures and euthanasia, including cell transplantations, were performed painlessly or under anesthesia, and within the strict guidelines of the Experimental Animal Center of Niigata University School of Medicine.

Statistical analysis. Statistical differences were analyzed by paired Student's *t*-test (MS Excel), and a value of $P < 0.05$ was regarded as statistically significant.

Results

Mitochondrial expression and its loss of p14 on various lineages of cancer cells. Because the endogenous expression of

p14 in mitochondria in previous studies was restricted to a few tumor lines, we examined whether it is frequently observed in tumor cells of diverse origins. While loss of p14 expression was observed in PK8, BxPC3 (both pancreatic adenocarcinoma), MCF7 (breast cancer), LoVo (colon adenocarcinoma) and A549 (lung adenocarcinoma), mitochondrial p14 expression was detected in HeLa (uterine cervical carcinoma), PC-9 (lung adenocarcinoma), T47D (breast cancer), HT-29 (colon adenocarcinoma) and HAK-1B (hepatocellular carcinoma) cells with or without its nucleolar expression, which was corroborated by colocalization with HSP60 by immunofluorescence (Fig. 1a). To precisely confirm the mitochondrial expression (not only by immunofluorescence using the antibodies or Mitotracker as in former studies) we employed immunoelectron microscopy. It revealed that p14 is localized not to the outer membrane but the inside (likely at cristae) of mitochondria (Fig. 1b). In contrast to tumor cells, p14 is consistently expressed in mitochondria in all lineages of normal (non-

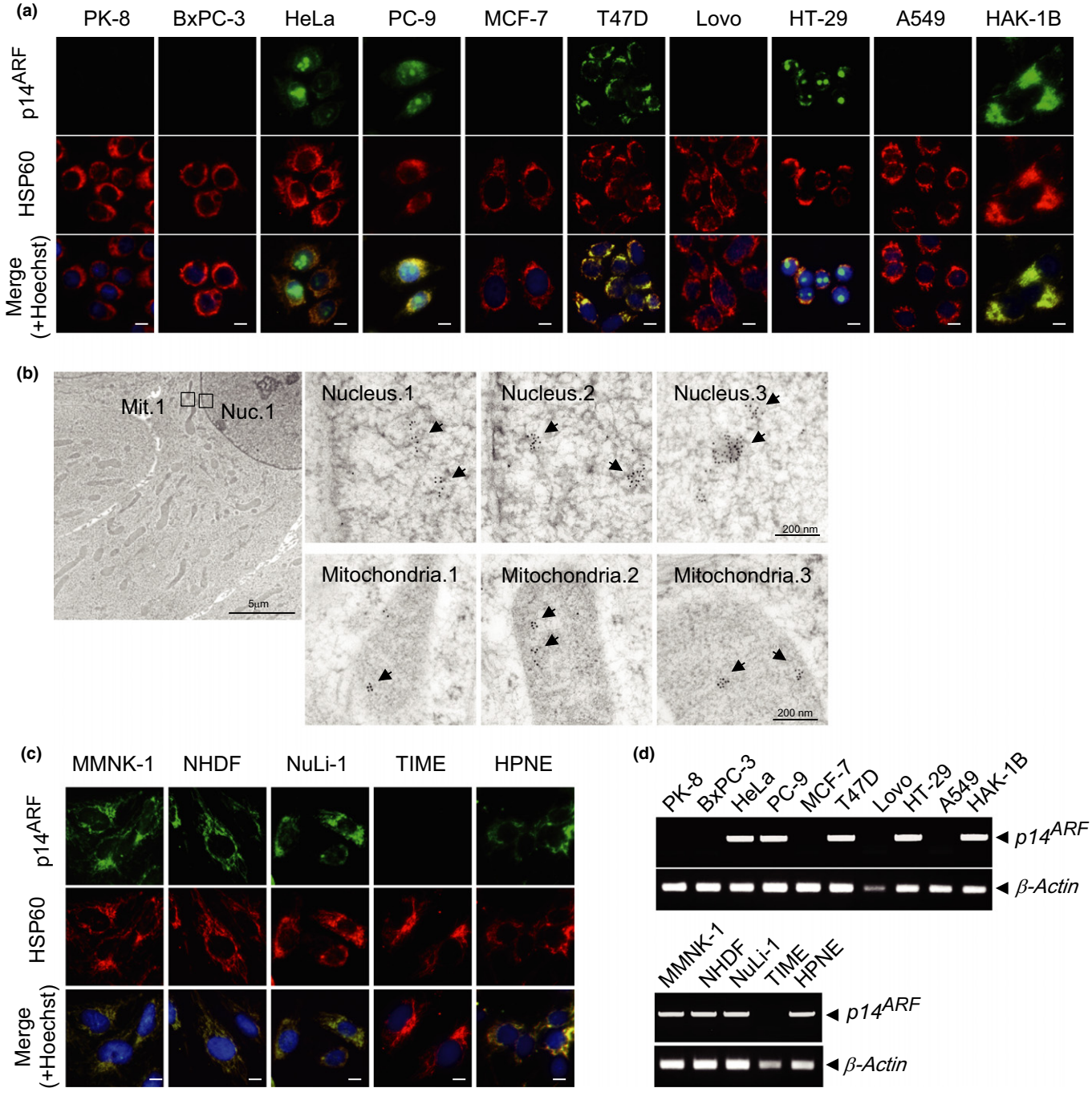

Fig. 1. Intracellular localization of endogenous $p14^{ARF}$ in tumor cells of diverse origins and non-neoplastic cells. (a) Double immunofluorescence using both anti-$p14^{ARF}$ (1:500 dilution) and anti-HSP60 (1:2000 dil.) antibodies for various lineages of human tumor cells. (b) Immunoelectron microscopy for HeLa cells using rabbit anti-p14 polyAb (1:100 dil.) and 10 nm gold particle-conjugated goat anti-rabbit IgG polyAb. (c) Double immunofluorescence for non-neoplastic cells of normal origins expressing p14 and HSP60. (d) Expression of endogenous *$p14^{ARF}$* both in the tumor cells and normal lineage cells by RT-PCR. β-actin was amplified as an endogenous control to *p14* mRNA.

neoplastic) cells examined, including MMNK-1 (cholangiocyte), NHDF (dermal fibroblast), NuLi-1 (brochial epithelium) and HPNE (pancreatic duct epithelium), but not TIME (vascular endothelium) (Fig. 1c). The mRNA expression in each cell line including tumor cells and non-neoplastic cells corresponded to that of p14 protein, respectively (Fig. 1d).

Design and mitochondrial targeting of the p14 MIS peptide. We previously defined the primary functional region, within the entire amino acid sequence encoded by $p14^{ARF}$, as "APAAVALVLMLLRSQRLGQQPLPRRPG," from the amino acid position of 38th (alanin) to position 65 (glycine); it functions as a growth inhibitory peptide when combined with the cell-penetrating polyarginine (nine D-Arginines; r9) domain, against gefitinib-resistant lung adenocarcinoma cells.[15] To bolster the antitumor action of this prototype, we first inserted the cathepsin B-cleavable motif "GFLG"[16] between the cell-penetrating domain and the p14 amino acid sequence in order to release the functional p14 sequence and to maximally exert its inhibitory effect following intracellular incorporation. This design was influenced by the fact that cathepsin B, one of the

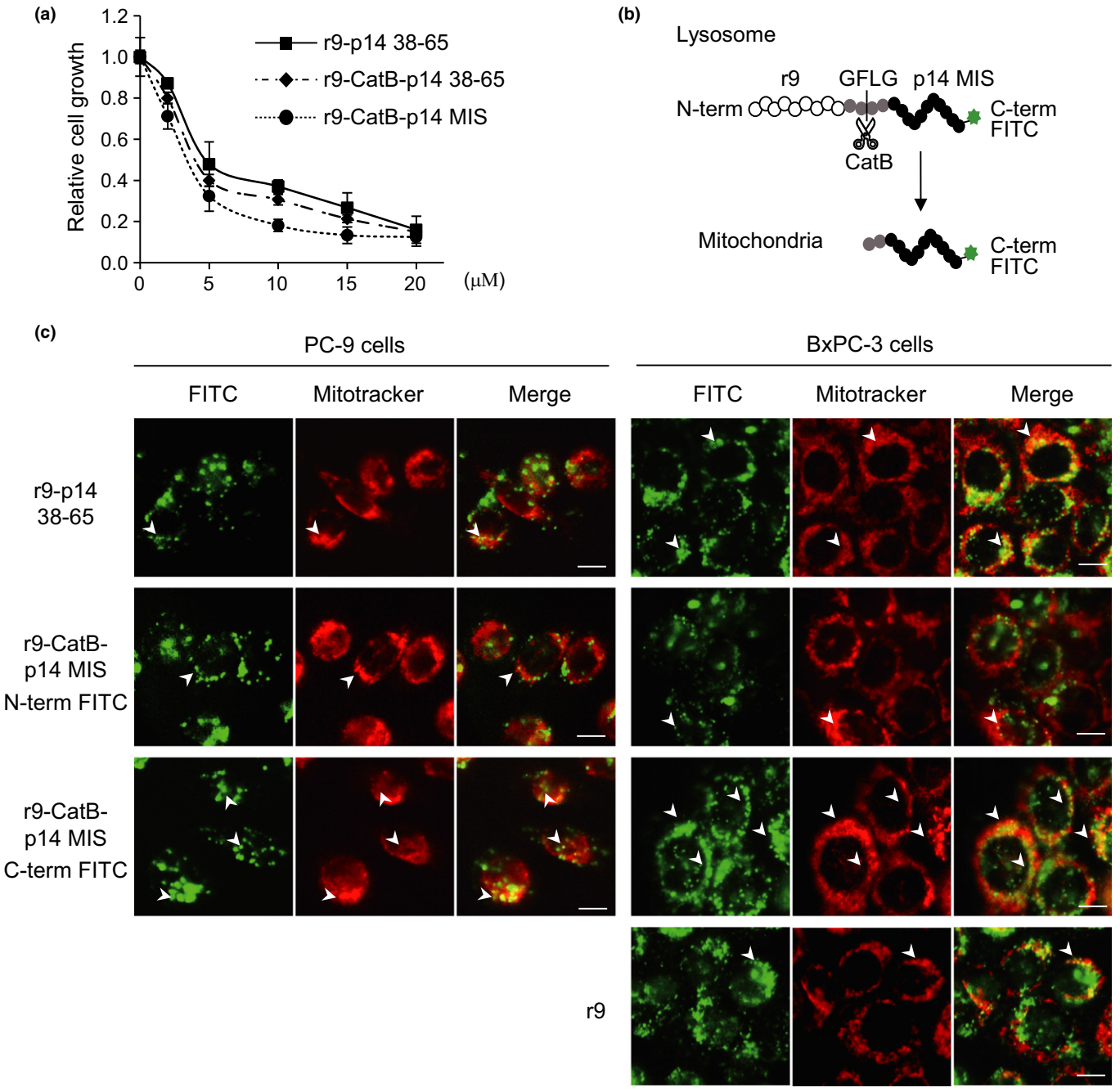

Fig. 2. Functional design of the mitochondrially-targeted growth inhibitory peptide originating from $p14^{ARF}$. (a) Efficiency of growth suppression of BxPC3 cells by the peptide harboring the minimal inhibitory sequence (MIS; covering the 45th to 56th amino acid) of p14 protein in comparison with longer sequence (38th to 65th a.a.) of p14, with the "GFLG," cathepsin B-cleavable motif as a spacer. (b) Design of the r9-p14 MIS peptide conjugated with FITC. (c) Mitochondrial localization of the cleavable r9-p14 MIS with N-terminal or C-terminal conjugation of FITC in comparison with the non-cleavable prototype p14 38-65 peptide. Mitochondrial localization was confirmed by colocalization with Mitotracker.

lysosomal cysteine proteases of the papain family, is highly activated in tumor cells.[17,18] We next attempted to shorten the sequence of the prototype peptide to the minimal functional amino acid sequence within the p14 derived segment. Because "AVAL," at the 41st through 44th amino acid positions of the p14 protein, is known to be the mitochondrial localization motif,[11] we constructed the truncated peptides with or without this motif, and compared the efficiency of

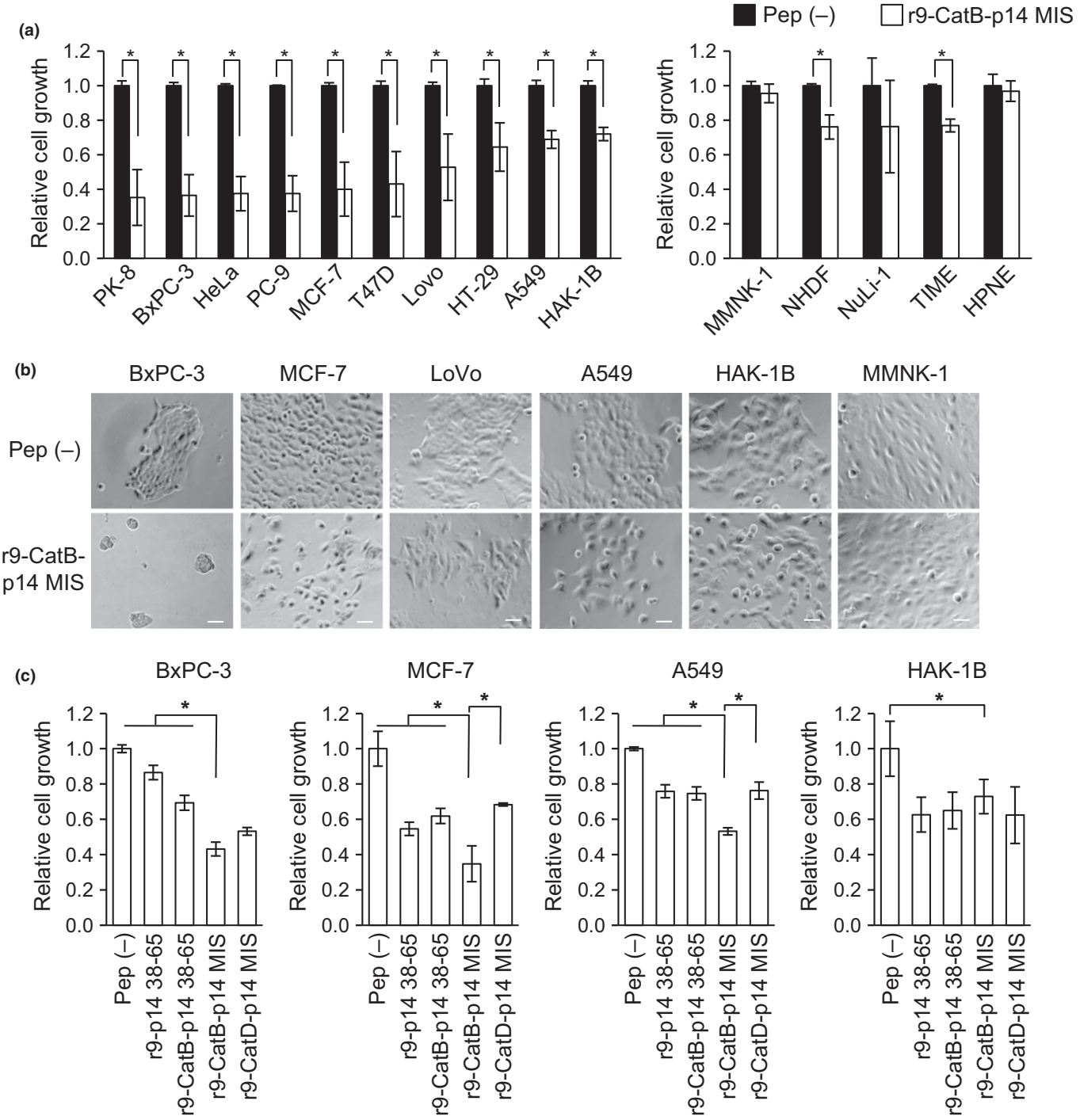

Fig. 3. *In vitro* challenge by the p14 MIS peptide (r9-CatB-p14 MIS) against various tumor cell lineages and normal cells of several different origins. (a) Growth suppression of tumor lines (1×10^5 cells) by 10 μM of the peptide 48 h after peptide introduction. Pancreas adenocarcinoma lines (PK-8, BxPC-3), uterine squamous cell carcinoma (HeLa), lung adenocarcinoma (PC-9, A549), breast adenocarcinoma (MCF-7, T47D), colon adenocarcinoma (LoVo, HT-29) and hepatocellular carcinoma (HAK-1B). The result of non-neoplastic cells, MMNK-1, NHDF, NuLi-1, TIME and HPNE, as described in the Materials and Methods, are shown. Means and SD of triplicates are shown. (b) Microscopic cellular image of growth alteration of the 10-μM peptide-treated tumor cells corresponding to the result shown in (a). (c) Magnitude of growth suppression by each inhibitory peptide (10 μM) with different designs (protease-cleavable spacer sequence and p14 sequence) on four malignant tumor lines of distinct origins. MTT assays were performed 48 h after peptide introduction.

growth suppression among the four peptides; namely, prototype r9-p14 38-65 with the original "GPG" *spacer*, *r9-CatB-p14 38-65* with the "GFLG" spacer, truncated r9-CatB-p14 41-57 retaining "AVAL," and the most truncated form, r9-CatB-p14 MIS (see Results and Fig. S1a). To evaluate the growth suppression by these four p14 peptides, the lung adenocarcinoma lines, both gefitinib-sensitive PC-9 and gefitinib-resistant RPC-9 clones, were employed for the treatment because they were already demonstrated to be very responsive to the original form, the r9-p14 38-65 peptide, in our previous study.[15]

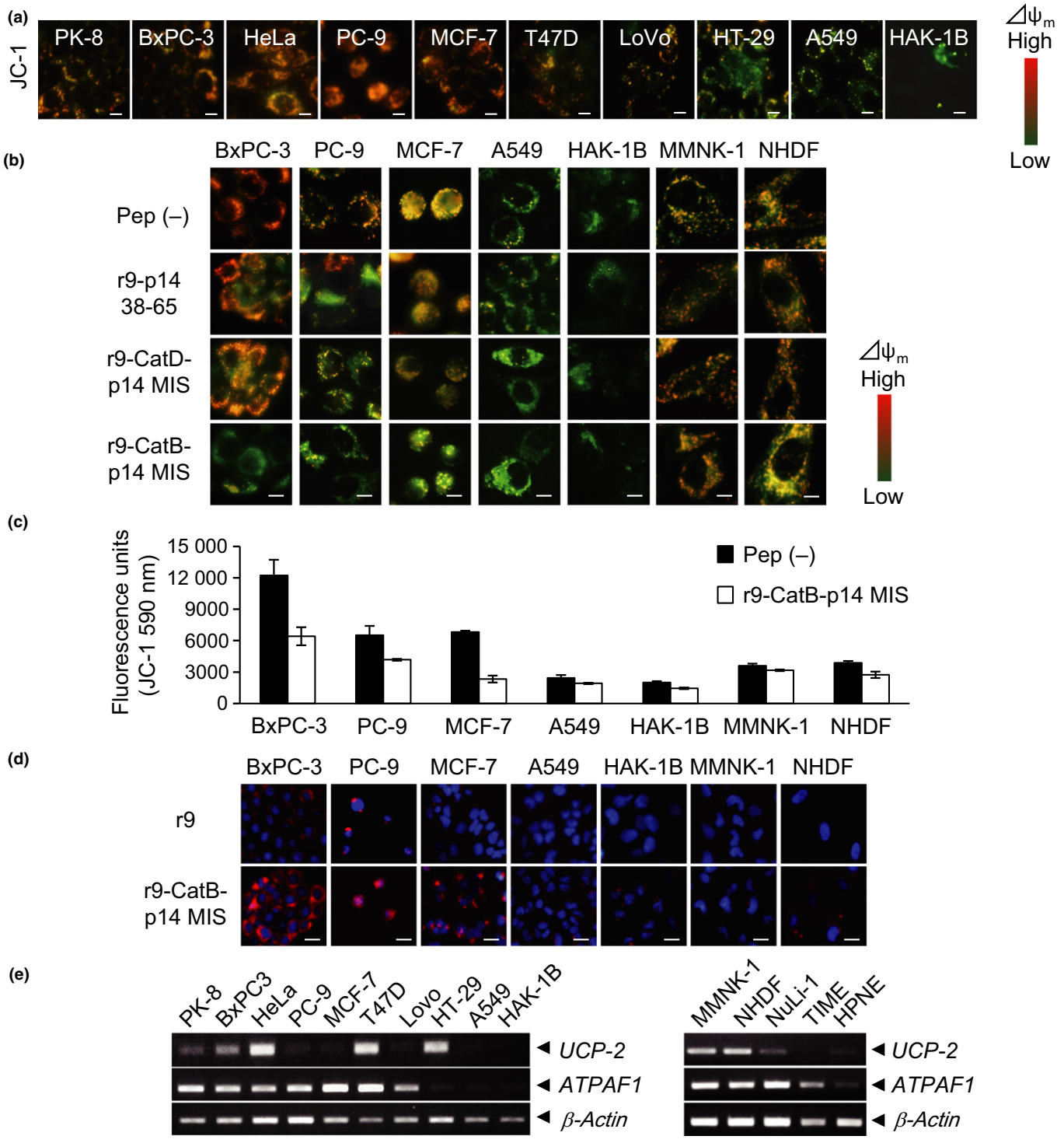

Fig. 4. r9-CatB-p14 MIS peptide functions to downregulate mitochondrial membrane potential (ΔΨm) of the tumor cells based on JC-1 dye staining. (a) Native proliferative status of ΔΨm detected by JC-1 in tumor and non-neoplastic cells. (b) Significant reduction of ΔΨm on tumor cells triggered by introducing 10 μM of r9-CatB-p14 MIS. (c) Quantitative analysis of fluorescence reduction in JC-1 staining in response to 10 μM of p14 MIS peptide. Means and SD of triplicates are shown. (d) Generation of ROS in the peptide-sensitive tumor cells. (e) RT-PCR evinced expression of the mitochondrial function-related gene, ATPAF1 and UCP-2, in tumor lines and non-neoplastic cells employed in the peptide study.

In the MTT assay, the most potent inhibition was obtained with r9-CatB-p14 MIS, the shortest form (Fig. S1b). It showed 80% inhibition of PC-9 and 85% inhibition of RPC-9 at a 10-μM concentration, which raised the inhibition 1.9 to 2.5-fold compared to the original r9-p14 38-65 peptide (Figs 2a,S1b). Taking all these results together, the most efficient amino acid sequence of the peptide was decided in rrrrrrrrr-GFLG-LVLMLLRSQRLG (r; D-Arg), named "r9-GFLG-p14 MIS," as shown in Figures 2(b) and S1a. Indeed, when r9-CatB-p14 MIS was introduced to tumor cells, PC-9 and BxPC3, it was more efficiently targeted to mitochondrias inside tumor cells. This was demonstrated by intracellular localization of the fluorescence signal derived from the FITC-labeled peptides 24 h after their introduction, as shown in Figure 2(c). Specifically, only a small proportion of the N-term FITC labeled original form "r9-p14 38-65" having Gly-Pro-Gly as a spacer, a non-cleavable form by cathepsin B, was localized to mitochondria as well as N-term FITC-labeled r9-CatB-p14 MIS (Fig. 2c, upper panel), while most of the rest of the r9-p14 38-65 was predominantly localized not to mitochondrias, but to lysosomes (Fig. 2c, lower panel). Thus, the C-terminal FITC-labeled r9-CatB-p14 MIS was prominently localized to mitochondria after tumor cell uptake. The result indicated that p14 MIS sequence is targeted to mitochondria after its cellular entry, and the cathepsin B-cleavable site (GFLG) promotes efficient mitochondrial localization of the cleaved p14 MIS sequence by isolating the r9 domain. Consequently, r9-CatB-p14 MIS is revealed to be the most efficient form of the p14-derived antitumor peptide that facilitates mitochondrial localization for potent inhibition of tumor cell growth (Fig. S2).

Challenge of the r9-CatB-MIS antitumor peptide against tumor cells of diverse origin *in vitro*. Upon finding that the peptide is properly recruited to the mitochondria after cellular entry, the anti-proliferative effect on tumor cells of several lineages was examined, insofar as the $p14^{ARF}$ gene is frequently inactivated or downregulated in various malignancies.[19] 10 μM of the r9-CatB-p14 MIS was introduced to each tumor line and the non-neoplastic cells, respectively, and the effect on cellular growth was evaluated by measuring the OD of both the untreated and the peptide-treated sample using the MTT assay. It successfully localized to mitochondria in all lineage of cells 24 h after the peptide treatment (Fig. S2). Consequently, some tumor lines including the pancreatic cancer and breast cancer lines (PK-8, BxPC3, HeLa, PC-9, MCF-7 and T47D) showed potent growth arrest between 60% and 65% in response to the peptide at the 10-μM concentration, whereas the tumor lines such as colon adenocarcinomas (LoVo, HT-29) and other lineages, such as A549 and HAK-1B, responded weakly (Fig. 3a, left graph). In contrast, non-neoplastic cells originating from cholangiocytes (MMNK-1), dermal fibroblast (NHDF), bronchial epitelium (Nuli-1), vascular endothel (TIME) and HPNE cells were not seriously affected in proliferation by the peptide treatment at the same concentration (Fig. 3a, right graph). Macroscopically, most of the peptide-sensitive tumor cells failed to form the prominent tumor nest and started to enter apoptosis after 48 h of peptide incubation, as seen with BxPC3 and MCF-7, while less sensitive lines such as LoVo, A549 and HAK-1B, and non-neoplastic line MMNK-1 were more viable and less decelerated for growth (Fig. 3b). This observation was more prominent for the peptide-treated cells at higher concentration (20 μM of r9-CatB-p14 MIS) (Fig. S3). Thus, not only the efficiency of mitochondrial localization, but pronounced tumor cell growth blockade was concordantly attained with r9-CatB-p14 MIS among prepared peptides spanning the proteolytic motif, and longer sequence, of the p14, establishing r9-CatB-p14 MIS as the most optimal design for the p14 tumor suppressor peptide (Fig. 3c).

Downregulation of mitochondrial membrane potential by the p14 peptide. To investigate the cellular function of the r9-CatB-p14 MIS after incorporation in the host, we focused initially on the mitochondrial effect of the peptide. Lipophilic cationic probe 5,5′,6,6′-tetrachloro-1,1′,3,3′-tetraethylbenzimidazolcarbocyanine iodide (JC-1), was utilized to monitor the mitochondrial membrane potential (Delta psi m; ΔΨm), where the color of the JC-1 dye specifically and reversibly changes from greenish orange to green as the mitochondrial membrane depolarizes.[20] The difference, ΔΨm, indicated by the JC-1 dye was examined among 10 tumor cell lines in the native proliferative condition (Fig. 4a). Treatment of tumor cells with 10 μM of the peptide induced a significant orange-to-green shift in JC-1, especially among the peptide-sensitive tumor cells (BxPC3, PC-9 and MCF-7), suggesting hindrance of normal mitochondrial function and triggering of apoptosis in these cells (Fig. 4b,c). In contrast, in the p14 peptide-resistant tumor cells such as A549 and HAK-1B, no appreciable change was detected on account of the very low ΔΨm in the native condition, indicating that their proliferation is less dependent on mitochondrial regulation. In the case of non-neoplastic cell lineages, ΔΨm is uniformly high and unaffected by the peptide (Fig. 4b,c). Downregulation of ΔΨm triggered by the peptide introduction ultimately led to reactive oxygen species (ROS) production in peptide-sensitive cells (Fig. 4d). Our original theory was that tumor cell sensitivity to the r9-CatB-p14 MIS peptide was mainly due to the loss of $p14^{ARF}$ expression because this peptide is supposed to restore *p14* tumor suppressor functions. However, some of the exceptional cell lines defied this notion: as shown in Figure 1(d), HeLa, PC-9 and T47D retaining p14 expression were still highly responsive, while p14-negative LoVo and A549 were less sensitive. A screen for expression of several mitochondrial genes, ATP synthase mitochondrial F1 complex assembly factor 1 (*ATPAF1*), which regulates activity of ATP synthase,[21] a key provider of ATP energy for cellular activity, was directly indicative of tumor sensitivity to the p14 peptide (Fig. 4e).

Sequence analysis and amplification of the peptide sensitivity in the resistant tumor cells. Because the amino acid sequence "LVMLLLRSQRLG" encoded between the 45th to 56th positions of the $p14^{ARF}$ protein has a three leucine ("blue lettered" L) stretch in a canonical position at a four amino acid interval, we examined whether this leucine positioning is critical for its antitumor function, by replacement with alanine (A) or glycine (G), where these amino acids may contribute to emulating helical structure (Fig. 5a). These derivatives, AAA and L50G, did not significantly affect peptide-resistant tumor cells, HAK-1B, but BxPC3 cells showed patterns of hampered growth and form consistent with the original inhibitory function indicating the unnecessity of forming helix by these keucines (Fig. 5b). Because Cyclosporin A (CsA), a representative immunosuppressant, is recognized to increase ΔΨm,[22] we treated the peptide-resistant HAK-1B cells with 1 μM of CsA prior to introduction of the r9-CatB-p14 MIS, and evaluated the effect of co-treatment. Treatment of HAK-1B with CsA prominently increased ΔΨm in HAK-1B, while ΔΨm was not significantly altered in the BxPC3 that originally showed high ΔΨm (Fig. 5c). CsA treatment restored growth suppression by the r9-CatB-p14 MIS in the peptide-resistant HAK-1B cells, from 25% inhibition up to 60% inhibition, an efficacy on a par with the peptide-sensitive BxPC3 cells (Fig. 5d). Substantial change

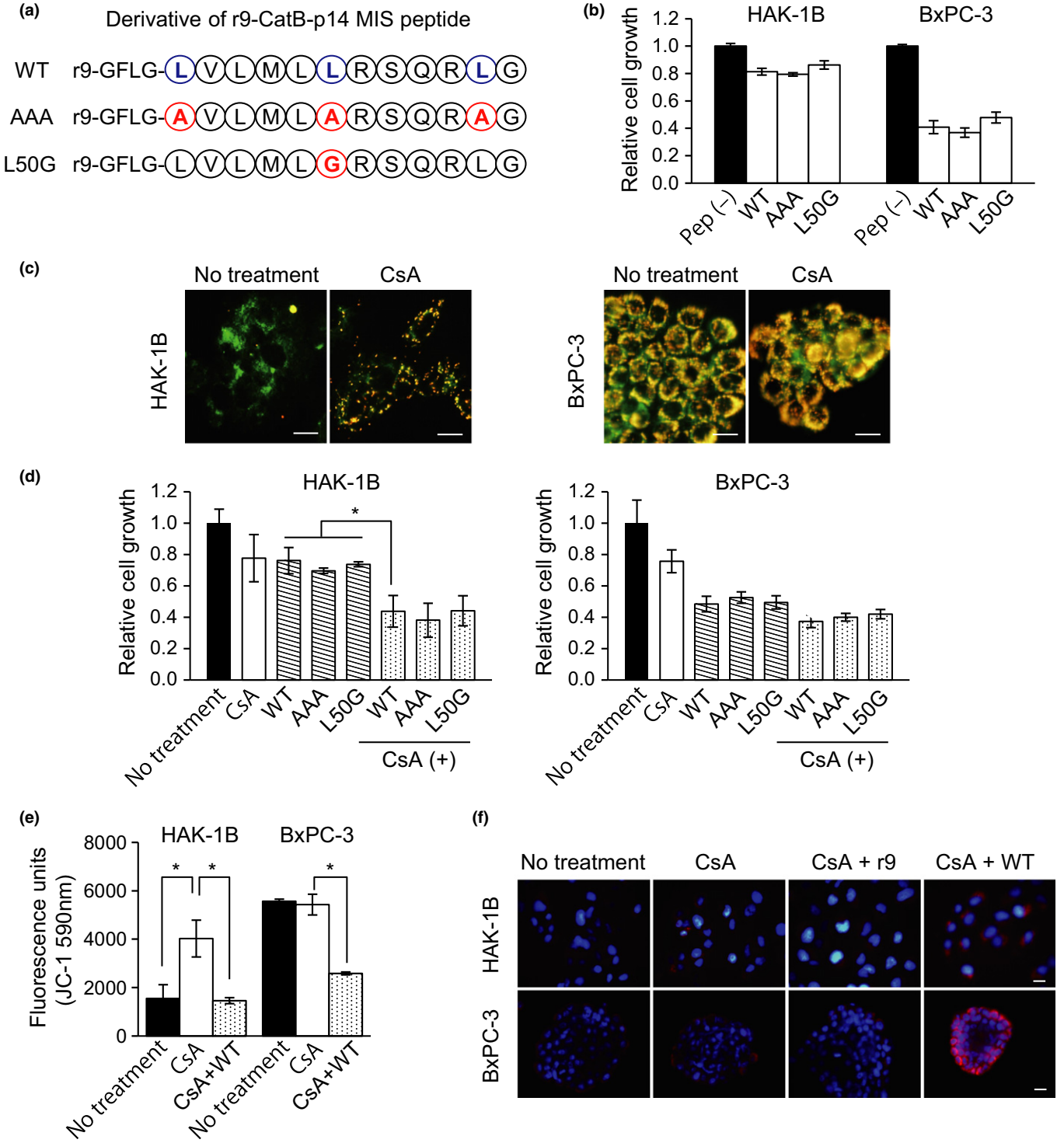

Fig. 5. Cyclosporin A potentiates the growth inhibitory effect of the p14 MIS peptide. (a) Structural perspective of the amino acid sequence of the p14 MIS; substitution of the three leucines (blue) within the original sequence of r9-CatB-p14 MIS with alanine or glycine (red). (b) MTT assay of the peptide-insensitive cell (HAK-1B) and sensitive cell (BxPC-3) for the wild type (WT) and two derivertive peptides. Means and SD of triplicates are shown. (c) Pretreatment with 1 μM of CsA potentiated the ΔΨm in the insensitive tumor cells HAK-1B; lack of significant enhancement by CsA in BxPC-3 cells. (d) Quantitative analysis of the growth inhibitory effect by CsA treatment on each peptide-treated cell by MTT assays. (e) Alteration of cellular JC-1 staining fluorescence representing ΔΨm in response to the combinatorial treatment with the p14 MIS peptide (10 μM) and CsA (1 μM) for the insensitive (HAK-1B) and sensitive (BxPC-3) tumor cells. (f) Increased production of ROS in cells treated by the p14 peptide in combination with CsA (CsA+WT).

in ΔΨm was quantitatively shown between the cells cotreated by CsA with the peptide and the cells treated by CsA alone (Fig. 5e). By contrast, downregulation of ΔΨm and growth suppression by the same treatment were minimized in several lineages of non-neoplastic cells except in the case of NuLi-1 (Fig. S4a–c). Mitochondrial dysfunction by the combinatorial

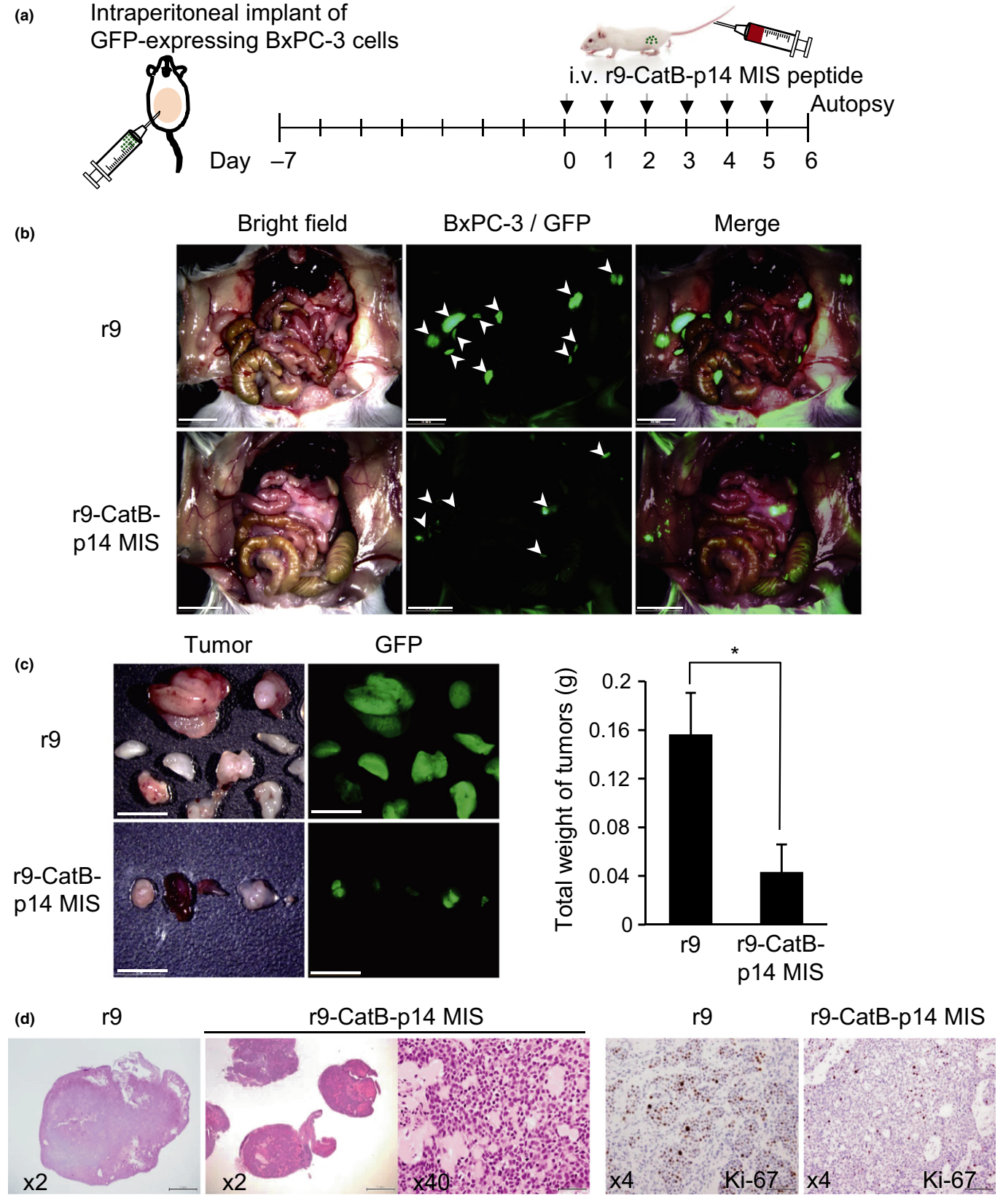

Fig. 6. Tumor suppression *in vivo* by the p14 MIS peptide. (a) The therapeutic protocol for tumor-bearing mice with repeated intravenous peptide administration. GFP-expressing BxPC-3 cells were allowed to grow intraperitoneally for a week before peptide-treatment. (b) *In vivo* distribution of metastatic tumors in the mouse abdominal cavity with or without the peptide treatment; upper row, an example of mice treated with control peptide (r9 alone); lower row, mouse treated with r9-CatB-p14 MIS. (c) GFP imaging of the intraperitoneal metastatic tumors collected from each mouse model treated with r9 alone or with r9-CatB-p14 MIS; the total weight of collected tumors per mouse from each group. (d) Histological examination of the tumor tissue sections from each peptide-treated mouse model. HE stain and immunohistochemistry using Ki-67 antibody.

treatment of CsA and the r9-CatB-p14 MIS yielded generation of reactive oxygen species (Fig. 5f).

Tumor suppression *in vivo* by transduction of r9-CatB-p14 MIS. Based on the *in vitro* functional assay of r9-CatB-p14 MIS, the mouse tumor model xenografted with stable GFP-expressing BxPC3 cells was prepared and subjected to an administration regimen for *in vivo* challenge by the peptide (Fig. 6a). Before moving to the therapeutic experiment, we first confirmed that r9-CatB-p14 MIS was delivered to the tumor tissue by detecting a fluorescent signal of the FITC-labeled peptide *in vivo* (Fig. S5). Mice were kept without therapeutic treatment for a week after intraperitoneal implantation of 2×10^6 of the tumor cells, allowing the growth of tumor cells *in vivo*. One week later, each mouse was intravenously administrated 300 μg of the r9-CatB-p14 MIS peptide per day, 6 days in total, then mice were autopsied on the day next to the last treatment. As shown in the fluorescence image of the peritoneal cavity, multiple GFP-positive disseminated tumor foci were observed (Fig. 6b, arrow head) in the peptide-treated mouse as well as in the control peptide consisting of the nine poly-D-arginine sequence (r9) alone (Fig. 6b). However, each tumor focus was significantly smaller in size, and the total weight of the intraperitoneally grown tumors with the peptide treatment was only one-quarter (i.e. 75% inhibition of tumor growth) that of the control peptide-treated mouse (Fig. 6c). Macroscopically visualized nodules were histologically confirmed as the adenocarcinoma lesions originating from implanted human BxPC3 cells. Consistent with the tumor growth suppression by the peptide, mitotically active cancer cells were rarely observed in the tumor tissue treated by r9-CatB-p14 MIS peptide (Ki-67-positivity was <1% in total number of cells), whereas prominent mitotic activity was detected in approximately 50% of Ki-67-positive tumor cells in the control tumor tissue treated with cell-penetrating domain, r9, alone (Fig. 6d).

Discussion

The tumor suppressor gene, $p14^{ARF}$, functions to halt cell division and trigger apoptosis in response to various oncogenic stresses in normal cells. Reflecting its indispensable role in prevention of tumor development, loss of the function through mutation or epigenetic silencing is observed in most forms of human cancer. As a canonical pathway, the $p14^{ARF}$ protein is recognized to activate p53 tumor suppressor by antagonizing an E3 ubiquitin ligase, MDM2. However, recent studies about another aspect of $p14^{ARF}$,which interacts with certain proteins other than MDM2, are exposing its novel p53-independent tumor suppressor activities.[2] In particular, mitochondrial p14 protein have been recently gained much attention that suggests novel function of p14 in contrast to conventional p14 function in nucleus.[11,12,23,24]

In this study, we first examined endogenous p14 expression in a spectrum of tumor cell lineages, some of which showed loss or marked downregulation of p14 expression; we then investigated the mitochondrial expression of p14 with or without its conventional nuclear/nucleoular expression in p14-positive tumor cells (Fig. 1a,d). Employing immunoelectron microscopy, we further corroborated the intramitochondrial localization of $p14^{ARF}$ as direct evidence of p14 localization at the mitochondrial inner membrane and at the matrix (Fig. 1b).

We previously identified the functional core sequence within the entire $p14^{ARF}$ ORF, which enables targeting of the *p14* gene product to mitochondrias to trigger apoptosis in tumor cells. From the previous findings, we next sought a more efficient and practical mitochondrial targeting system against tumor cells using the potent antitumor peptide "r9-CatB-p14 MIS." This tumor suppressor peptide encodes the minimal inhibitory amino acid sequence "LVLMLLRSQRLG" derived from the 45th to 56th amino acid position of $p14^{ARF}$, which successfully targeted itself to mitochondria with the catepsin B-cleavable motif "GFLG" as a spacer, and strongly suppressed the hyperactivity of tumor mitochondria, indicated by downregulation of ΔΨm. Previously, "AVAL" was reporetd to be the hypothetical mitochondrial localization motif.[11] In this study, the r9-CatB-p14 MIS lacking "AVAL" significantly showed mitochondrial localization. Thus, the MIS sequence seems to be sufficient and these four amino acids are revealed to be dispensable for mitochondrial migration.

The magnitude of growth inhibition by the p14 MIS peptide was initially expected to be dependent on the loss of expression of mitochondrial p14 in tumor cells; that is, the peptide was expected to be highly effective in tumors lacking endogenous p14 expression. However, the potent growth inhibition by p14 MIS peptide was obtained not only in p14-negative tumor lines (e.g. PK8, BXPC3 and MCF-7) but also in p14-expressing lines, such as PC-9 (Figs 1d,3a), which provokes questions on the precise molecular mechanisms of tumor-selective growth suppression by the candidate peptide. Recognizing that a point of action for the p14 MIS peptide is the regulation of the mitochondrial membrane depolarization (downreguration of ΔΨm), we screened for prospective molecules relating possibly to mitochondrial activation, and retrieved "*ATPAF1*," ATP synthase mitochondrial F1 complex assembly factor 1,[21] which critically correlated with sensitivity of tumor cells to r9-CatB-p14 MIS peptide (Fig. 4e). Although the p14 MIS peptide amino acid sequence predicts a functional α-helical structure in view of a triple leucine run at a five residue interval, substitution of these leucines with alanine (A) or glycine (G)

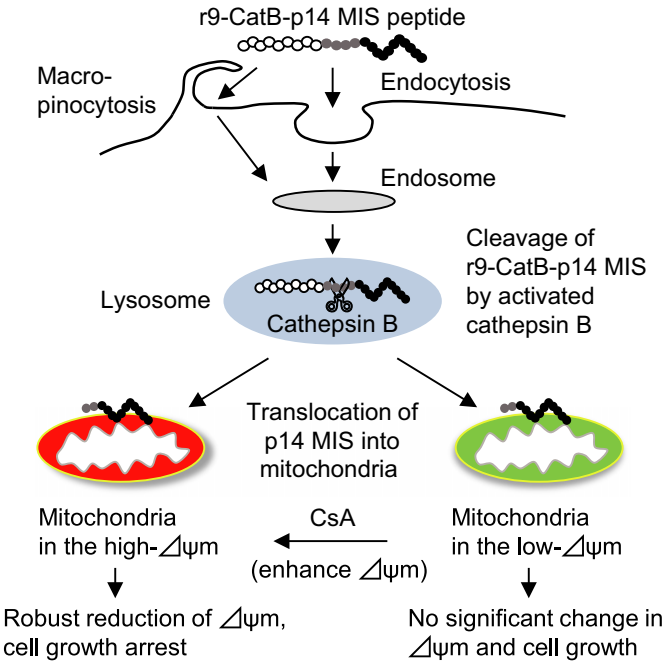

Fig. 7. Action mode of r9-CatB-p14 MIS peptide. Intracellularly incorporated peptide localizes to lysosome via endosome, then released by cathepsin B-cleavable motif and migrates to mitochondria to alter ΔΨm on tumor cells.

did not affect the original function of the p14 peptide, as variants AAA and L50G also showed comparable growth suppression to the original peptide (WT) (Fig. 5a,b). This suggests that the peptide does not functionally require the predicted helix arrangement for its intracellular function, contrary to usual expectations.

The investigated anti-tumor peptide, r9-CatB-p14MIS, as shown in the scheme summarizing the mode of its action (Fig. 7), offers two unique advantages in that the peptide automatically transits to mitochondria after intracellular entry and functions to downregulate the hyper-activated $\Delta\Psi m$ in neoplastic cells, inducing growth arrest and/or triggering apoptosis in diverse tumor cell lineages without appreciably affecting non-neoplastic cells. Growth inhibition by the p14 MIS was consistently observed, particularly in cancer cells with a high $\Delta\Psi m$ (up to 70% inhibition at 10 μM peptide), probably due to selective sensitivity for reduction of $\Delta\Psi m$. p14 MIS response of tumor cells with native low $\Delta\Psi m$ potential was weaker than that of the tumor cells with high $\Delta\Psi m$; however, cotreatment with cyclosporine A and p14 MIS significantly augmented the inhibitory effect in these low responders (e.g. there was a threefold enhancement [from 20% to 60%] in HAK-1B hepatoma cells [Fig. 5c–f]). We then sought *in vivo* tumor suppression using the r9-CatB-p14MIS peptide on tumor-bearing mice. First, the FITC-labeled peptide by intravenous administration showed successful accumulation in the multiple pancreatic adenocarcinoma lesions in the peritoneal cavity (Fig. S5).

The antitumor effect after six repeated administrations based on the therapeutic protocol with daily peptide injection (300 μg/i.v./day) resulted in approximately 75% inhibition of tumor growth compared with that of r9 alone-treated group (Fig. 6b,c). Consistent with macroscopic tumor regression, histology of the peptide-treated tumor evinced a marked decrease in number of Ki-67 antigen-positive cells compared to the control r9-treated tumors (Fig. 6d).

Recent advances in nanotechnology have yielded important clues toward countering malignant tumors, and functional oligopeptides appear to offer strong potential as effective biologics, wherein their dwindling scales (approximately 3–5 kDa in molecular weight) are consistent with the miniaturization efforts of nanobiology. In this study, we attempted to develop a novel antitumor peptide, r9-CatB-p14 MIS, and explore its application for peptide-based tumor therapeutics. The peptide showed dramatic growth suppression against intraperitoneally disseminated tumors by downregulating mitochondrial $\Delta\Psi m$, while being intrinsically non-invasive to normal tissues *in vivo* and suggesting a safe physiologic compatibility for clinical applications, on the strength of its derivation from the $p14^{ARF}$ tumor suppressor protein sequence.

Accumulated molecular biological studies indicate that the mitochondrion is a crucial organelle in determining cell fate, and is, therefore, a burgeoning focus of interest in cancer therapeutics.[25] While our future studies will direct increasing attention to the underlying molecular interaction mechanisms, we believe that our present report as such will offer critical insights for treating malignancies using peptide-based molecular agents targeting tumor cell mitochondria, and add significantly to frontline biomedical strategies against cancer.

Acknowledgments

The authors are grateful to Dr Kyl Myrick for critical reading of the manuscript. We are also thankful to Professor Nagio Takigawa (Kawasaki Medical School), Professor Katsuyuki Kiura (Okayama University) and Professor Hirohisa Yano (Kurume University) for providing lung and liver cancer lines. This research was supported by Grant-in-Aid for Scientific Research on Innovative Areas No. 25670263 (E. K.) from the Japan Society for the Promotion of Science.

Disclosure Statement

The authors have no conflict of interest to declare.

References

1 Quelle DE, Zindy F, Ashmun RA, Sherr CJ. Alternative reading frames of the INK4a tumor suppressor gene encode two unrelated proteins capable of inducing cell cycle arrest. *Cell* 1995; **83**: 993–1000.
2 Sherr CJ. Divorcing ARF and p53: an unsettled case. *Nat Rev Cancer* 2006; **6**: 663–73.
3 Weber JD, Kuo ML, Bothner B *et al.* Cooperative signals governing ARF-mdm2 interaction and nucleolar localization of the complex. *Mol Cell Biol* 2000; **20**: 2517–28.
4 Rizos H, McKenzie HA, Ayub AL *et al.* Physical and functional interaction of the p14ARF tumor suppressor with ribosomes. *J Biol Chem* 2006; **281**: 38080–8.
5 Dominguez-Brauer C, Chen YJ, Brauer PM, Pimkina J, Raychaudhuri P. ARF stimulates XPC to trigger nucleotide excision repair by regulating the repressor complex of E2F4. *EMBO Rep* 2009; **10**: 1036–42.
6 Abida WM, Gu W. p53-Dependent and p53-independent activation of autophagy by ARF. *Cancer Res* 2008; **68**: 352–7.
7 Serrano M, Lee HW, Chin L, Cordon-Cardo C, Beach D, DePinho RA. Role of the INK4a locus in tumor suppression and cell mortality. *Cell* 1996; **85**: 27–37.
8 Kamijo T, Zindy F, Roussel MF *et al.* Tumor suppression at the mouse INK4a locus mediated by the alternative reading frame product p19ARF. *Cell* 1997; **91**: 649–59.
9 Kamijo T, Bodner S, van de Kamp E, Randle DH, Sherr CJ. Tumor spectrum in ARF-deficient mice. *Cancer Res* 1999; **59**: 2217–22.
10 Itahana K, Bhat KP, Jin A *et al.* Tumor suppressor ARF degrades B23, a nucleolar protein involved in ribosome biogenesis and cell proliferation. *Mol Cell* 2003; **12**: 1151–64.
11 Irvine M, Philipsz S, Frausto M *et al.* Amino terminal hydrophobic import signals target the p14(ARF) tumor suppressor to the mitochondria. *Cell Cycle* 2010; **9**: 829–39.
12 Pimkina J, Murphy ME. Interaction of the ARF tumor suppressor with cytosolic HSP70 contributes to its autophagy function. *Cancer Biol Ther* 2011; **12**: 503–9.
13 Fahraeus R, Lain S, Ball KL, Lane DP. Characterization of the cyclin-dependent kinase inhibitory domain of the INK4 family as a model for a synthetic tumour suppressor molecule. *Oncogene* 1998; **16**: 587–96.
14 Kondo E, Saito K, Tashiro Y *et al.* Tumour lineage-homing cell-penetrating peptides as anticancer molecular delivery systems. *Nat Commun* 2012; **3**: 951–63.
15 Saito K, Takigawa N, Ohtani N *et al.* Antitumor impact of p14ARF on gefitinib-resistant non-small cell lung cancers. *Mol Cancer Ther* 2013; **12**: 1616–28.
16 Shankar R, Samykutty A, Riggin C, Kannan S, Wenzel U, Kolhatkar R. Cathepsin B degradable star-shaped peptidic macromolecules for delivery of 2-methoxyestradiol. *Mol Pharm* 2013; **10**: 3776–88.
17 Gondi CS, Rao JS. Cathepsin B as a cancer target. *Expert Opin Ther Targets* 2013; **17**: 281–91.
18 Iacobuzio-Donahue CA, Shuja S, Cai J, Peng P, Murnane MJ. Elevations in cathepsin B protein content and enzyme activity occur independently of glycosylation during colorectal tumor progression. *J Biol Chem* 1997; **272**: 29190–9.
19 Geradts J, Wilentz RE, Roberts H. Immunohistochemical [corrected] detection of the alternate INK4a-encoded tumor suppressor protein p14(ARF) in archival human cancers and cell lines using commercial antibodies: correlation with p16 (INK4a) expression. *Mod Pathol* 2001; **14**: 1162–8. Erratum in: *Mod Pathol* 2002; **15**: 76.

20 Smiley ST, Reers M, Mottola-Hartshorn C *et al.* Intracellular heterogeneity in mitochondrial membrane potentials revealed by a J-aggregate-forming lipophilic cation JC-1. *Proc Natl Acad Sci USA* 1991; **88**: 3671–5.
21 Wang ZG, White PS, Ackerman SH. Atp11p and Atp12p are assembly factors for the F(1)-ATPase in human mitochondria. *J Biol Chem* 2001; **276**: 30773–8.
22 Cassarino DS, Swerdlow RH, Parks JK, Parker WD Jr, Bennett JP Jr. Cyclosporin A increases resting mitochondrial membrane potential in SY5Y cells and reverses the depressed mitochondrial membrane potential of Alzheimer's disease cybrids. *Biochem Biophys Res Commun* 1998; **248**: 168–73.
23 Milojkovic A, Hemmati PG, Müer A *et al.* p14ARF induces apoptosis via an entirely caspase-3-dependent mitochondrial amplification loop. *Int J Cancer* 2013; **133**: 2551–62.
24 Reef S, Zalckvar E, Shifman O *et al.* A short mitochondrial form of p19ARF induces autophagy and caspase-independent cell death. *Mol Cell* 2006; **22**: 463–75.
25 Ralph SJ, Rodríguez-Enríquez S, Neuzil J, Saavedra E, Moreno-Sánchez R. The causes of cancer revisited: "mitochondrial malignancy" and ROS-induced oncogenic transformation – why mitochondria are targets for cancer therapy. *Mol Aspects Med* 2010; **31**: 145–70.

Supporting Information

Additional Supporting Information may be found online in the supporting information tab for this article:

Fig. S1. Amino acid sequence of designed p14 peptides and their effect on growth suppression of the tumor cells.

Fig. S2. Colocalization of r9-CatB-p14 MIS with the lysosomal or mitochondrial markers in tumor cells after its intracellular incorporation.

Fig. S3. Growth suppression and induction of apoptosis in the p14 peptide-treated tumor cells.

Fig. S4. Cyclosporin A (CsA) potentiates mitochondrialmembrane potential.

Fig. S5. *In vivo* uptake of the r9-CatB-p14 MIS peptide via intravenous administration.